Science Advances
AAAS

Supplementary Materials for

Chiral Kondo lattice in doped $MoTe_2/WSe_2$ bilayers

Daniele Guerci *et al.*

Corresponding author: Daniele Guerci, danieleguerci@hotmail.it

Sci. Adv. **9**, eade7701 (2023)
DOI: 10.1126/sciadv.ade7701

This PDF file includes:

These supplementary materials contain the details of analytic calculations as well as additional numerical details supporting the results presented in the main text.

The Kondo lattice Hamiltonian

In this section we detail the connection between the tight-binding model and the Schrieffer-Wolff transformation to obtain the Kondo lattice Hamiltonian given in the main text.

The tight-binding Hamiltonian

Assuming W-layer weakly correlated the tight-binding Hamiltonian that describes the low-energy properties of the system reads $H = H_0 + H_W + H_t$:

$$\begin{aligned} H_0 =& -\frac{\Delta}{2}(N_{Mo} - N_W) + U\sum_{\mathbf{r}\in Mo} n_{\mathbf{r}\uparrow}n_{\mathbf{r}\downarrow} \\ H_W =& -t_W \sum_{\langle \mathbf{r},\mathbf{r}'\rangle \in W} e^{-i\nu_{\mathbf{r},\mathbf{r}'}2\pi\sigma/3} c^\dagger_{\mathbf{r}\sigma}c_{\mathbf{r}'\sigma}, \\ H_t =& -t_{Mo}\sum_{\langle \mathbf{r},\mathbf{r}'\rangle \in Mo} f^\dagger_{\mathbf{r}\sigma}f_{\mathbf{r}'\sigma} - t_h \sum_{\langle \mathbf{r},\mathbf{r}'\rangle} f^\dagger_{\mathbf{r}}c_{\mathbf{r}'}. \end{aligned} \tag{1}$$

We have introduced the operator $f_{\mathbf{r}\sigma}$ for the Mo and $c_{\mathbf{r}\sigma}$ for W-layer, respectively. We notice that differently from H_0 and H_W the contribution H_t changes the local configuration in the Mo layer.

The Schrieffer-Wolff transformation

We assume that U is the largest energy scale, $U \gg t_{Mo}$, and $\Gamma(\epsilon_F)/\Delta < 1$ where $\Gamma(\epsilon_F)$ is the hybridization function:

$$\Gamma(\epsilon_F) = \pi t_h^2 \rho(\epsilon_F)\langle V^*_{\mathbf{k}}V_{\mathbf{k}}\rangle_{FS} = \pi t_h^2 \left(\frac{3\sqrt{3}a_M^2}{8\pi^2}\right)\oint_{FS} dk_t \frac{V^*_{\mathbf{k}}V_{\mathbf{k}}}{|\nabla_{\mathbf{k}}\epsilon_{\mathbf{k}\sigma}|}. \tag{2}$$

Fig. S1 show the evolution of $\Gamma(\epsilon_F)$ as a function of the filling x for the value of t_h^2/Δ corresponding to $J_K/t_W = 1$ value used for the numerical calculations shown in the manuscript. Within these assumptions valence fluctuations in Mo layer are suppressed. We now observe that the tunneling H_t can be decomposed as:

$$H_t = \sum_{q=-1}^{1}\sum_{d=-1}^{1} T_{q,d}, \tag{3}$$

where $T_{q,d}$ gathers all tunneling events that change the number of electrons unbalance between Mo and W by q and the double occupancies in Mo layer by d. We list the $T_{q,d}$ operators below:

$$\begin{aligned}
T_{+1,+1} &= -t_h \sum_{\mathbf{r}\in Mo}\sum_{\sigma}\sum_{j=1}^{3} n_{\mathbf{r}\bar{\sigma}} f^{\dagger}_{\mathbf{r}\sigma} c_{\mathbf{r}+\boldsymbol{\delta}_j\sigma}, \\
T_{+1,0} &= -t_h \sum_{\mathbf{r}\in Mo}\sum_{\sigma}\sum_{j=1}^{3} h_{\mathbf{r}\bar{\sigma}} f^{\dagger}_{\mathbf{r}\sigma} c_{\mathbf{r}+\boldsymbol{\delta}_j\sigma}, \\
T_{0,+1} &= -t_{Mo} \sum_{\mathbf{r}\in Mo}\sum_{\sigma}\sum_{j=1}^{3} \left[n_{\mathbf{r}\bar{\sigma}} f^{\dagger}_{\mathbf{r}\sigma} f_{\mathbf{r}+\boldsymbol{\gamma}_j\sigma} h_{\mathbf{r}+\boldsymbol{\gamma}_j\bar{\sigma}} + n_{\mathbf{r}+\boldsymbol{\gamma}_j\bar{\sigma}} f^{\dagger}_{\mathbf{r}+\boldsymbol{\gamma}_j\sigma} f_{\mathbf{r}\sigma} h_{\mathbf{r}\bar{\sigma}} \right], \\
T_{0,0} &= -t_{Mo} \sum_{\mathbf{r}\in Mo}\sum_{\sigma}\sum_{j=1}^{3} \left[n_{\mathbf{r}\bar{\sigma}} f^{\dagger}_{\mathbf{r}\sigma} f_{\mathbf{r}+\boldsymbol{\gamma}_j\sigma} n_{\mathbf{r}+\boldsymbol{\gamma}_j\bar{\sigma}} + h_{\mathbf{r}\bar{\sigma}} f^{\dagger}_{\mathbf{r}\sigma} f_{\mathbf{r}+\boldsymbol{\gamma}_j\sigma} h_{\mathbf{r}+\boldsymbol{\gamma}_j\bar{\sigma}} + h.c. \right],
\end{aligned} \tag{4}$$

we notice that $T_{-q,-d} = T^{\dagger}_{q,d}$, $n_{\mathbf{r}\sigma} = f^{\dagger}_{\mathbf{r}\sigma} f_{\mathbf{r}\sigma}$ and $h_{\mathbf{r}\sigma} = 1 - n_{\mathbf{r}\sigma}$. Moreover, the terms $T_{-1,+1}$ and $T_{+1,-1}$ vanish. Before moving on, we notice that the intralayer hopping H_{Mo} does not change the charge imbalance $N_{Mo} - N_W$ ($q = 0$), i.e. H_{Mo} commutes with $N_{Mo} - N_W$ ($[N_{Mo} - N_W, H_{Mo}] = 0$). Moreover, $[N_{Mo} - N_W, T_{q,d}] = 2qT_{q,d}$ and

$$\sum_{\mathbf{r}\in Mo} [n_{\mathbf{r}\uparrow} n_{\mathbf{r}\downarrow}, T_{q,d}] = dT_{q,d}. \tag{5}$$

We seek an unitary transformation $U = \exp(-iS)$ which eliminates hops between states with different numbers of doubly occupied sites and interlayer charge imbalance [33, 34, 57]:

$$\bar{H} \equiv e^{iS} H e^{-iS} = H + [iS, H] + \frac{[iS, [iS, H]]}{2!} + \cdots, \tag{6}$$

where we applied the Baker-Campbell-Haussdorf formula. We now notice that to the lowest order in the expansion we have:

$$[H_0, iS] = \sum_{q,d}^{(q,d)\neq 0} T_{q,d}, \tag{7}$$

where in previous sum we exclude the term with $q = 0$ and $d = 0$ in shorthand notation $(q, d) \neq 0$. We readily realize that the solution of Eq. (7) reads:

$$S = -i \sum_{q,d}^{(q,d)\neq 0} \frac{T_{q,d}}{dU - q\Delta}. \tag{8}$$

From the latter expression we find:

$$\bar{H} = H_0 + T_{0,0} + H_W + \frac{1}{2} \sum_{q,d}^{(q,d)\neq 0} \sum_{q',d'}^{(q',d')\neq 0} \frac{[T_{q,d}, T_{q',d'}]}{-q\Delta + dU} + \sum_{q,d}^{(q,d)\neq 0} \frac{[T_{q,d}, H_W + T_{0,0}]}{-q\Delta + dU} + O([H_W + T_{0,0}]S^2). \tag{9}$$

Projecting the model in the low-energy subspace with one-electron in Mo layer, i.e. $n_{\mathbf{r}} = 1$ for $\mathbf{r} \in Mo$, we find that the latter term vanishes. Furthermore, the projection constraints $q' = -q$ and $d' = -d$:

$$\bar{H} = -t_W \sum_{\langle \mathbf{r},\mathbf{r}'\rangle \in W} e^{-i\nu_{\mathbf{r},\mathbf{r}'} 2\pi s_\sigma/3} c^{\dagger}_{\mathbf{r}\sigma} c_{\mathbf{r}'\sigma} - \mu N_W + \frac{1}{2} \sum_{q,d}^{(q,d)\neq 0} \frac{[T_{q,d}, T_{-q,-d}]}{dU - q\Delta}, \tag{10}$$

where the constant energy term $\Delta N_W/2$ has been absorbed in the chemical potential shift and $T_{0,0}$ vanishes in the low-energy subspace. By performing straightforward calculations we find that the commutator in Eq. (10) gives:

$$\begin{aligned}
\frac{1}{2} \sum_{q,d}^{(q,d)\neq 0} \frac{[T_{q,d}, T_{-q,-d}]}{dU - q\Delta} =& t_h^2 \left(\frac{1}{\Delta} + \frac{1}{U - \Delta} \right) \sum_{\mathbf{r}\in Mo} \sum_{jl=1}^{3} \boldsymbol{S}_{\mathbf{r}} \cdot c^{\dagger}_{\mathbf{r}+\boldsymbol{\delta}_j\sigma} \boldsymbol{\sigma}_{\sigma\sigma'} c_{\mathbf{r}+\boldsymbol{\delta}_l\sigma'} + \frac{4t_{Mo}^2}{U} \sum_{\langle \mathbf{r},\mathbf{r}'\rangle \in A} \boldsymbol{S}_{\mathbf{r}} \cdot \boldsymbol{S}_{\mathbf{r}'} \\
&+ t_h^2 \left(\frac{1}{\Delta} - \frac{1}{U - \Delta} \right) \sum_{\mathbf{k}} |V_{\mathbf{k}}|^2 c^{\dagger}_{\mathbf{k}} c_{\mathbf{k}}.
\end{aligned} \tag{11}$$

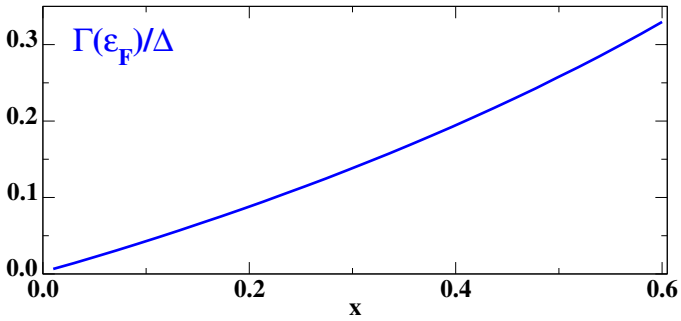

Figure S1. **Hybridization function**. Evolution of $\Gamma(\epsilon_F)/\Delta$ as a function of the filling x of the conduction band.

Expanding close to the bottom of the conduction band [$\kappa(\kappa')$ for $\uparrow$ ($\downarrow$)] $|V_{\kappa/\kappa'+\mathbf{k}}|^2 \simeq 9(a_M k)^2/4$ we realize that the latter terms can be simply accounted by a redefinition of the bare mass $m_W \to m_W/[1+(t_h/\Delta - t_h/(U-\Delta))t_h/(2t_W)]$. Finally, we find the effective spin-fermion Hamiltonian:

$$\bar{H} = \sum_{\mathbf{k}} \xi_{\mathbf{k}\sigma} c^\dagger_{\mathbf{k}\sigma} c_{\mathbf{k}\sigma} + J_H \sum_{\langle \mathbf{r},\mathbf{r}'\rangle \in A} \boldsymbol{S}_{\mathbf{r}} \cdot \boldsymbol{S}_{\mathbf{r}'} + \frac{1}{2N} \sum_{\mathbf{r}\in \mathrm{Mo}} \sum_{\mathbf{k},\mathbf{p}} e^{-i(\mathbf{k}-\mathbf{p})\cdot \mathbf{r}} J_{\mathbf{k},\mathbf{p}} \boldsymbol{S}_{\mathbf{r}} \cdot c^\dagger_{\mathbf{k}\sigma} \boldsymbol{\sigma}_{\sigma\sigma'} c_{\mathbf{p}\sigma'}, \tag{12}$$

where $J_H = 4t^2_{Mo}/U$, $J_{\mathbf{k},\mathbf{p}} = J_K V^*_{\mathbf{k}} V_{\mathbf{p}}$, $J_K = 2t_h^2[1/\Delta + 1/(U-\Delta)]$, $\xi_{\mathbf{k}\sigma} = \epsilon_{\mathbf{k}\sigma} - \epsilon_F$, $\epsilon_{\mathbf{k}\sigma}$ is the electron dispersion and ϵ_F fixes the number of electron in the conduction band. The dispersion relation reads $\epsilon_{\mathbf{k}\sigma} = -2t_W \sum_{j=1}^3 \cos(\mathbf{k}\cdot \boldsymbol{a}_i + 2\pi s_\sigma/3)$, $\boldsymbol{a}_1 = \sqrt{3} a_M (1,0)$, $\boldsymbol{a}_{2,3} = \sqrt{3} a_M \left(-1/2, \pm\sqrt{3}/2\right)$ are the lattice vectors with $a_M = 5$nm the moiré cell lattice constant. The form factor is $V_{\mathbf{k}} = \sum_{j=1}^3 e^{i\mathbf{k}\cdot\boldsymbol{\delta}_j}$. Despite U is large and J_H small the particular form of the exchange interaction $J_{\mathbf{k},\mathbf{p}} = J_K V^*_{\mathbf{k}} V_{\mathbf{p}}$ gives rise to a non-trivial competition between a low-density magnetic phase and a paramagnetic heavy Fermi liquid. We observe that in the following we will measure the value of Δ with respect to the bottom of conduction band $-6t_W$.

On the higher-order corrections

Higher order corrections in the expansion lower the symmetry of the spin interaction in the Mo-layer. This can be simply realized noticing that the phase factor in the Hamiltonian H_W lower the spin-symmetry of the model to $U(1)$ around z. Including higher-order hopping processes mediated by t_h gives an XXZ spin model with Dzyaloshinskii–Moriya interactions:

$$H_S = J_H \sum_{\langle \mathbf{r},\mathbf{r}'\rangle \in \mathrm{Mo}} \left(S^z_{\mathbf{r}} S^z_{\mathbf{r}'} + \gamma S^+_{\mathbf{r}} S^-_{\mathbf{r}'} + h.c.\right) + D \sum_{\langle \mathbf{r},\mathbf{r}'\rangle \in \mathrm{Mo}} \left(\boldsymbol{S}_{\mathbf{r}} \times \boldsymbol{S}_{\mathbf{r}'}\right)_z, \tag{13}$$

we refer to Ref. [8] for additional details. For simplicity we consider the isotropic limit $\gamma = 1/2$ and $D = 0$ in our calculations.

The mean-field approach

In this section we detail the mean-field of Abrikosov fermions discussed in the main text. We perform the decomposition of the spin-1/2 into spinons $\boldsymbol{S}_{\mathbf{r}} = \chi^\dagger_{\mathbf{r}\alpha} \boldsymbol{\sigma}_{\alpha\beta} \chi_{\mathbf{r}\beta}/2$ and performing the mean-field decomposition in the magnetic and excitonic channels we obtain the mean-field Hamiltonian:

$$\begin{aligned}
\bar{H}_{\mathrm{mf}} =& \lambda \sum_{\mathbf{k}} \chi^\dagger_{\mathbf{k}} \chi_{\mathbf{k}} + \frac{h^z}{2} \sum_{\mathbf{k}} \chi^\dagger_{\mathbf{k}} \sigma^z \chi_{\mathbf{k}} + \frac{h^\parallel}{2} \sum_{\mathbf{k}} \left[\chi^\dagger_{\mathbf{k}+\mathbf{Q}} \sigma^- \chi_{\mathbf{k}} + h.c.\right] + \sum_{\mathbf{k}\sigma} \xi_{\mathbf{k}\sigma} c^\dagger_{\mathbf{k}\sigma} c_{\mathbf{k}\sigma} \\
&+ \frac{M^z}{2} \sum_{\mathbf{k}} J_{\mathbf{k},\mathbf{k}} c^\dagger_{\mathbf{k}} \sigma^z c_{\mathbf{k}} + \frac{M^\parallel}{2} \sum_{\mathbf{k}} \left[J_{\mathbf{k}+\mathbf{Q},\mathbf{k}} c^\dagger_{\mathbf{k}+\mathbf{Q}} \sigma^- c_{\mathbf{k}} + h.c.\right] \\
&+ J_K \sum_{\mathbf{k}} \left[V^*_{\mathbf{k}} \Phi^* c^\dagger_{\mathbf{k}} \chi_{\mathbf{k}} + h.c.\right].
\end{aligned} \tag{14}$$

In the previous expression M^z and $M^\parallel$ are the out-of-plane and in-plane components of the magnetization of the local moments, the magnetic field h^z and $h^\parallel$ are given by:

$$\begin{aligned} h^z &= 6M^z + \sum_{\mathbf{p}} J_{\mathbf{p},\mathbf{p}} \langle c^\dagger_{\mathbf{p}} \sigma^z c_{\mathbf{p}} \rangle / N, \\ h^\parallel &= -3M^\parallel + \sum_{\mathbf{p}} \left(J_{\mathbf{p},\mathbf{p}+\mathbf{Q}} \langle c^\dagger_{\mathbf{p}} \sigma^+ c_{\mathbf{p}+\mathbf{Q}} \rangle + h.c. \right) / (2N). \end{aligned} \tag{15}$$

The excitonic order parameter reads:

$$\Phi = -\sum_{\mathbf{k}} V^*_{\mathbf{k}} \langle c^\dagger_{\mathbf{k}} \chi_{\mathbf{k}} \rangle / (2N). \tag{16}$$

The mean-field free-energy reads:

$$\begin{aligned} F_{\rm mf} =& -k_B T \sum_{\mathbf{k}} \sum_{\lambda} \log \left[1 + e^{-E_{\mathbf{k}\lambda}/k_B T} \right] + 2J_K N |\Phi|^2 + \frac{3J_H N}{2} {M^\parallel}^2 \\ & - 3J_H N M^{z\,2} - J_K M^z N m^z - J_K N M^\parallel m^\parallel - \lambda N + N\mu x, \end{aligned} \tag{17}$$

where $E_{\mathbf{k}\lambda}$ is the mean-field dispersion relation. The mean-field solution is obtained by minimizing $F_{\rm mf}$ with respect to the variational parameters $M^z, M^\parallel, \Phi, m^z, m^\parallel$. The Lagrange multiplier λ imposes the Gutzwiller constraint $\sum_{\mathbf{k}} \langle \chi^\dagger_{\mathbf{k}} \chi_{\mathbf{k}} \rangle / N = 1$, while the chemical potential μ fixes the number of particle in conduction band $\sum_{\mathbf{k}} \langle c^\dagger_{\mathbf{k}} c_{\mathbf{k}} \rangle / N = x$. Taking the saddle point of Eq. (17) with respect to the variational parameters gives a set of self-consistency equations that are solved by find-root algorithm.

Energetics of the HFL and AFM states

In this section we detail the weak coupling expansion to determines the characteristic energy scales of the AFM and HFL phases that are the RKKY energy and the Kondo temperature, respectively. We will also introduce the effective model describing the quasiparticle excitations in the two different regimes.

AFM

In the magnetic regime the local moments $\boldsymbol{S}_{\mathbf{r}}$ form a 120° AFM order with $\langle \boldsymbol{S}_{\mathbf{r}} \rangle = \left(M^\parallel \cos \mathbf{Q} \cdot \mathbf{r}, M^\parallel \sin \mathbf{Q} \cdot \mathbf{r}, M^z \right)$, $\mathbf{Q} = \kappa - \kappa'$, correspondingly the conduction electron Hamiltonian reads:

$$\bar{H}^c_{\rm mf} = \sum_{\mathbf{k}} \xi_{\mathbf{k}\sigma} c^\dagger_{\mathbf{k}\sigma} c_{\mathbf{k}\sigma} + \frac{J_K M^z}{2} \sum_{\mathbf{k}} |V_{\mathbf{k}}|^2 c^\dagger_{\mathbf{k}} \sigma^z c_{\mathbf{k}} + \frac{J_K M^\parallel}{2} \sum_{\mathbf{k}} \left[V^*_{\mathbf{k}} V_{\mathbf{k}+\mathbf{Q}} c^\dagger_{\mathbf{k}} \sigma^+ c_{\mathbf{k}+\mathbf{Q}} + h.c. \right]. \tag{18}$$

In the limit of low-doping the Fermi surface is a small electron pocket around $\kappa(\uparrow)$ and $\kappa'(\downarrow)$ that are folded into the origin of the magnetic Brillouin zone γ_m, depicted in Fig. S4(b). Expanding close to quadratic order around γ_m and keeping only the two lowest energy bands we find the continuum model:

$$\bar{\mathcal{H}}^c_{\rm mf} = \sum_{\mathbf{k}} c^\dagger_{\mathbf{k}} \left[\left(\frac{\hbar^2 k^2}{2m_W} - \epsilon_F \right) \sigma_0 + \frac{9 J_K a_M^2}{8} \sum_a d_a(\mathbf{k}) \sigma_a \right] c_{\mathbf{k}}, \tag{19}$$

where $d_z(\mathbf{k}) = M^z k^2$, $d_x(\mathbf{k}) = -M^\parallel (k_x^2 - k_y^2)$ and $d_y(\mathbf{k}) = 2M^\parallel k_x k_y$. We readily realize that due to the SOC term the spin is no longer a good quantum number, the eigenstates $|u_{\mathbf{k}\lambda}\rangle$ are labeled by $\lambda = \pm$ and the corresponding eigenvalues are $\epsilon_{\mathbf{k}\lambda} = (\hbar^2 k^2 / 2m_W - \epsilon_F) + \lambda 9 J_K a_M^2 k^2 |M| / 8$ with $|M| = \sqrt{(M^z)^2 + (M^\parallel)^2}$. We observe that the theory is O(3) invariant under rotation of the magnetization $M^a \to R_{ab} M^b$. The resulting stabilization energy does not depend on the orientation of the local moments. The Fermi momentum obtained by setting $\epsilon_{\mathbf{k}\lambda} = 0$ reads $k_F^\pm = \sqrt{2 m_\lambda \epsilon_F / \hbar^2}$ where $m_\lambda = m_W / [1 + \lambda (J_K / 8 t_W)]$ and the Fermi energy is $\epsilon_F \simeq x / \left(\sum_\lambda \rho_\lambda \right)$ with $\rho_\lambda = \rho_0 m_\lambda / m_W$. We notice that in the Kondo regime J_K is smaller than the bandwidth of conduction electrons $9 t_W$ so that the mass is always positive. The kinetic energy variation with respect to the normal state reads:

$$\delta \epsilon^c_{\rm mf} = \epsilon^c_{\rm mf} - \epsilon^c_{J_K = 0} = -\rho_0 \bar{J}_K^2 |M|^2 / 2, \tag{20}$$

where $\bar{J}_K$ is the average over the FS of the Kondo exchange. We conclude that the total energy per site in the magnetic regime is given by:

$$\epsilon_{\rm mf} = -3J_H|M|^2/2 - \rho_0 \bar{J}_K^2 |M|^2/2. \tag{21}$$

The energy gain from the coupling between the conduction band and the local moments goes quadratically in the electron density x. We conclude observing that interaction effects between conduction electrons in the B sublattice introduce the tendency to develop a finite out-of-plane ferromagnetic polarization. The analysis of the effect of interaction between conduction electrons is left to future studies.

HFL

In the paramagnetic regime electrons are described by the mean-field Hamiltonian reads:

$$\bar{H}_{\rm mf} = \sum_{\mathbf{k}\sigma} \xi_{\mathbf{k}\sigma} c^\dagger_{\mathbf{k}\sigma} c_{\mathbf{k}\sigma} + \lambda \sum_{\mathbf{k}} \chi^\dagger_{\mathbf{k}} \chi_{\mathbf{k}} + J_K \sum_{\mathbf{k}\sigma} \left[V^*_{\mathbf{k}} \Phi^* c^\dagger_{\mathbf{k}} \chi_{\mathbf{k}} + h.c. \right]. \tag{22}$$

We easily realize that the Green's function of the problem reads:

$$\boldsymbol{G}^{-1}_\sigma(\mathbf{k}, i\epsilon) = \begin{pmatrix} i\epsilon - \lambda & -J_K \Phi V_{\mathbf{k}} \\ -J_K \Phi^* V^*_{\mathbf{k}} & i\epsilon - \xi_{\mathbf{k}\sigma} \end{pmatrix}, \tag{23}$$

so that the saddle-point equation for the bosonic amplitude Φ can be written as:

$$\Phi = -\frac{T}{2N} \sum_{\mathbf{k}\sigma} \sum_{i\epsilon} V^*_{\mathbf{k}} \mathcal{G}_{\chi,\sigma}(\mathbf{k}, i\epsilon) J_K V_{\mathbf{k}} \Phi G_{c,\sigma}(\mathbf{k}, i\epsilon), \tag{24}$$

where $\mathcal{G}_{\chi,\sigma}(\mathbf{k}, i\epsilon) = (i\epsilon - \lambda)^{-1}$ is the bare Green's function and $G_{c,\sigma}(\mathbf{k}, i\epsilon) = [i\epsilon - \xi_{\mathbf{k}\sigma} - \Sigma_{c,\sigma}(\mathbf{k}, i\epsilon)]^{-1}$ with

$$\Sigma_{c,\sigma}(\mathbf{k}, i\epsilon) = J_K^2 |\Phi|^2 |V_{\mathbf{k}}|^2/(i\epsilon - \lambda). \tag{25}$$

From the latter expression we readily find the quasiparticle residue:

$$Z_{\mathbf{k}} = \frac{1}{1 - \partial_z \Sigma_{c,\sigma}(\mathbf{k}, z)|_{z=0}} = \frac{1}{1 + J_K^2 |\Phi|^2 V^*_{\mathbf{k}} V_{\mathbf{k}}/\lambda^2}. \tag{26}$$

The latter quantity evaluated at the Fermi surface of the heavy Fermi liquid gives the mass enhancement of the quasiparticles. Discarding the $\Phi = 0$ solution the equation reduces to

$$\frac{1}{J_K} = \frac{1}{2N} \sum_{\mathbf{k}\sigma} \frac{f(E_{\mathbf{k}-\sigma}) - f(E_{\mathbf{k}+\sigma})}{\sqrt{(\xi_{\mathbf{k}\sigma} - \lambda)^2 + 4J_K^2 |\Phi|^2 |V_{\mathbf{k}}|^2}} = \frac{1}{2N} \sum_{\mathbf{k}\sigma} \frac{\theta(-E_{\mathbf{k}-\sigma})}{\sqrt{(\xi_{\mathbf{k}\sigma} - \lambda)^2 + 4J_K^2 |\Phi|^2 |V_{\mathbf{k}}|^2}}, \tag{27}$$

where $E_{\mathbf{k}\pm} = (\xi_{\mathbf{k}\sigma} + \lambda)/2 \pm \sqrt{(\xi_{\mathbf{k}\sigma} - \lambda)^2 + 4J_K^2 |\Phi|^2 |V_{\mathbf{k}}|^2}/2$ and the RHS is obtained taking the we took the zero temperature limit and considering the case $x < 1$ where only the lower band is filled. In addition we also have the self-consistent equation for λ:

$$\frac{T}{N} \sum_{\mathbf{k}\sigma} \sum_{i\epsilon} \frac{1}{i\epsilon - \lambda - \Sigma_{\chi,\sigma}(\mathbf{k}, i\epsilon)} = 1 \implies \frac{1}{2N} \sum_{\mathbf{k}\sigma} \theta(-E_{\mathbf{k}-\sigma}) \left(1 + \frac{\xi_{\mathbf{k}\sigma} - \lambda}{\sqrt{(\xi_{\mathbf{k}\sigma} - \lambda)^2 + 4J_K^2 |\Phi|^2 |V_{\mathbf{k}}|^2}} \right) = 1. \tag{28}$$

The onset of the HFL instability is determined looking at the instability condition of the normal state to interlayer hybridization. In this case the solution of Eq. (28) is $\lambda = 0$, i.e. the local moments are pinned at the Fermi level, and Eq. (24) becomes:

$$\frac{1}{J_K} + \Pi^0_{\chi c}(\mathbf{q} \to 0, i\Omega = 0) = 0, \tag{29}$$

where $\Pi^0_{\chi c}(\mathbf{q} \to 0, \tau) = -\langle T_\tau(\hat{V}_{\mathbf{q}=0}(\tau) \hat{V}^\dagger_{\mathbf{q}=0}) \rangle/N$, $\hat{V}_{\mathbf{q}=0} = \sum_{\mathbf{k}} V^*_{\mathbf{k}} c^\dagger_{\mathbf{k}} \chi_{\mathbf{k}}/\sqrt{2}$ and $\Pi^0_{\chi c}(\mathbf{q} \to 0, i\Omega) = \int_0^\beta e^{i\Omega\tau} \Pi^0_{\chi c}(\mathbf{q} \to 0, \tau)$. Expanding close to the bottom of the band Eq. (29) becomes:

$$\frac{1}{J_K} - \frac{\rho_0}{2} \int_{\epsilon_F}^{E_\Lambda} d\epsilon \frac{|V_\epsilon|^2}{\epsilon - \epsilon_F} - \frac{\rho_0}{2} \int_0^{\epsilon_F} d\epsilon \frac{|V_\epsilon|^2}{\epsilon_F - \epsilon} = 0, \tag{30}$$

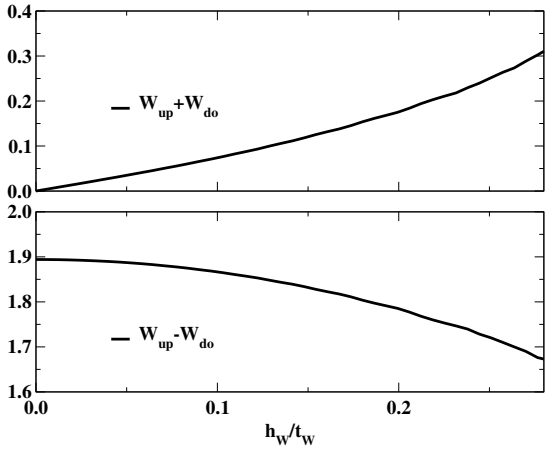

Figure S2. **Intrinsic topological response of the HFL.** Spin Hall effect (bottom panel) and anomalous Hall effect (top panel) in the HFL as a function of the Zeeman field. The calculation is performed at $J_K/t_W = 1$, $x = 0.65$.

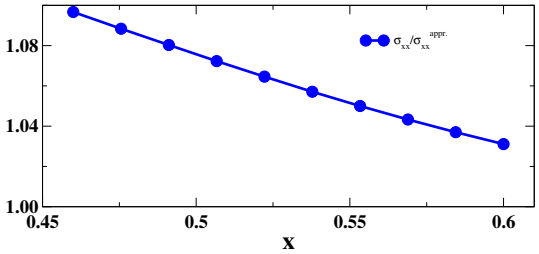

Figure S3. **Longitudinal conductivity.** Ratio between the numerical evaluation of Eq. (32) and $\sigma_{xx} = e^2\tau(1-x)/\bar{m}^*$ obtained assuming a circular Fermi surface with average velocity.

where $|V_\epsilon| = 9a_M^2 k_\epsilon^2/4$ with $k_\epsilon = \sqrt{2m_W\epsilon/\hbar^2}$.The integral is characterized by a log singularity at ϵ_F. We introduce the IR cutoff T_K, $\epsilon \to \epsilon \pm T_K$, that regularize the divergence. Finally, by performing simple calculations we find:

$$T_K \simeq \epsilon_F e^{-1/(\rho_0 \bar{J}_K)}. \tag{31}$$

Since the average over the Fermi surface $\bar{J}_K$ goes linearly with the doping x in conduction band we find that the Kondo temperature is exponentially suppressed in the limit $x \to 0^+$. Finally, we notice that the Fermi energy is proportional to the filling factor in the WSe_2 layer, $\epsilon_F \propto x$. Away from the low-doping regime of exponential suppression we have $T_K \propto x$ which is different from the conventional result $T_K \propto \sqrt{x}$. The behavior $m/m^* \sim T_K \propto x$ is consistent with experimental results in Ref. [56].

Transport properties

In this section we detail the evaluation of the transverse and longitudinal conductivities in the various phases of the phase diagram.

Charge transport in the HFL

In the paramagnetic regime the local moments fractionalize giving rise to a finite density of holes in $MoTe_2$ layer. In this regime the field $\Phi_{\mathbf{r}}$ is equivalent to the holon operator carrying physical charge -1 [50], i.e. opposite to the electron charge. As a result both conduction electrons c and spinon χ contribute to the charge current. Within the semiclassical Boltzmann equation approach and in the relaxation time approximation the transport properties are

simply obtained as integrals over the quasiparticle Fermi surface [48, 49]:

$$\sigma_{xx} = \frac{3\sqrt{3}a_M^2 e^2\tau}{8\pi^2}\sum_\sigma \oint_{FS} dk_t \frac{\bar{v}^x_{F,\sigma}\bar{v}^x_{F,\sigma}}{\hbar|\bar{\boldsymbol{v}}_{F,\sigma}|}, \tag{32}$$

and

$$\sigma_{xy} \equiv \sigma^{\rm Ohm}_{xy} + \sigma^{\rm AH}_{xy} = \frac{3\sqrt{3}a_M^2}{8\pi^2}\frac{e^3\tau^2 B}{\hbar}\sum_\sigma \oint_{FS} dk_t \frac{\bar{v}^y_{F,\sigma}\left[\bar{v}^y_{F,\sigma}\partial_{k_x} - \bar{v}^x_{F,\sigma}\partial_{k_y}\right]\bar{v}^x_{F,\sigma}}{\hbar|\bar{\boldsymbol{v}}_{F,\sigma}|} + \frac{e^2}{2\pi h}\sum_\sigma \oint_{FS} dk_t\, \boldsymbol{t}\cdot\boldsymbol{A}_\sigma(\mathbf{k}), \tag{33}$$

where the anomalous Hall contribution $\sigma^{\rm AH}_{xy}$ arises from the circulation of the Berry connection $\boldsymbol{A}_\sigma(\mathbf{k}) = i\langle u_{\mathbf{k}\sigma}|\partial_{k_a} u_{\mathbf{k}\sigma}\rangle$, with $|u_{\mathbf{k}\sigma}\rangle$ occupied eigenstate of the Hamiltonian in Eq. (22), along the FS. In Eqs. (32) and (33) k_t is the component of $\mathbf{k}$ along the tangent $\boldsymbol{t}$ to the FS curve. We notice that the FS of the heavy quasiparticle is obtained by the set of $\mathbf{k}$ points solution of the equation:

$$\text{heavy FS}: \xi_{\mathbf{k}\sigma} - J_K^2|\Phi|^2|V_{\mathbf{k}}|^2/\lambda = 0, \tag{34}$$

where the second term comes from the conduction electron self-energy $\Sigma_{c,\sigma}(\mathbf{k},0)$ introduced in Eq. (25) computed at $i\omega = 0$. The Fermi velocity $\boldsymbol{v}_{F,\sigma}$ is obtained replacing $\mathbf{k}\to\mathbf{k}+e\mathbf{A}(t)/\hbar$ in $\bar{\xi}_{\mathbf{k}\sigma} = Z_{\mathbf{k}\sigma}[\xi_{\mathbf{k}\sigma} - J_K^2|\Phi|^2|V_{\mathbf{k}}|^2/\lambda]$ and expanding to linear order around the FS we find $\bar{\xi}_{\mathbf{k}_F+\frac{e}{\hbar}\mathbf{A}(t)\sigma} \simeq e\bar{\boldsymbol{v}}_F\cdot\mathbf{A}(t)$ where:

$$\bar{\boldsymbol{v}}_{F,\sigma} = \frac{Z_{\mathbf{k}_F,\sigma}}{\hbar}\nabla_{\mathbf{k}}[\xi_{\mathbf{k}\sigma} - J_K^2|\Phi|^2|V_{\mathbf{k}}|^2/\lambda]\Big|_{\mathbf{k}_F}, \tag{35}$$

and $Z_{\mathbf{k},\sigma} = [1-\partial_z\Sigma_{c,\sigma}(\mathbf{k},z)|_{z=0}]^{-1}$ is the quasiparticle weight. The evaluation of σ_{xx} and $\sigma^{\rm Ohm}_{xy}$ is considerably simplified observing that the Fermi surface consists of a hole-pocket around $\boldsymbol{\kappa}'$ for spin $\uparrow$ and $\boldsymbol{\kappa}$ for spin $\downarrow$, respectively. Assuming a circular hole-like Fermi surface with average mass $\bar{m}^*$ the longitudinal contribution becomes

$$\sigma_{xx} = 2\frac{e^2\tau}{\bar{m}^*}\left(\frac{\sqrt{3}a_M^2}{8\pi^2}\right)k_F^2\int_0^{2\pi} d\phi\cos^2\phi = \frac{e^2\tau}{\bar{m}^*}\left(2\pi k_F^2\frac{\sqrt{3}a_M^2}{8\pi^2}\right) = \frac{e^2\tau(1-x)}{\bar{m}^*}. \tag{36}$$

As a sanity check we show in Fig. S3 the ratio between Eq. (36) and the numerical evaluation of Eq. (32) for various concentrations of electrons in the W-layer. By following the same line of reasoning we obtain $\sigma^{\rm Ohm}_{xy} = -e^3\tau^2 B(1-x)/\bar{m}^{*2}$. We now look at the anomalous contribution $\sigma^{\rm AH}_{xy}$ which can be conveniently written as $\sigma^{\rm AH}_{xy} = e^2(W_\uparrow + W_\downarrow)/h$ where $W_\sigma = \int d^2\mathbf{k} f(\epsilon_{\mathbf{k}\sigma})\Omega_\sigma(\mathbf{k})/(2\pi)$ and $\Omega_\sigma(\mathbf{k}) = \partial_{k_x}A^y_\sigma(\mathbf{k}) - \partial_{k_y}A^x_\sigma(\mathbf{k})$. Due to the opposite winding of spin $\uparrow$ and $\downarrow$ we find that in the absence of a magnetic field $W_\uparrow = -W_\downarrow$. We observe that the difference $W_\uparrow - W_\downarrow$ gives a finite spin Hall (SH) conductivity [40] even in the absence of the external field. Fig. S2 shows $W_\uparrow \pm W_\downarrow$ as a function of the magnetic field at doping $x = 0.46$ and $J_K/t_W = 1$. The small value of $W_\uparrow + W_\downarrow$ at finite B follows from the Berry curvature distribution which is peaked around the bare FS of the conduction electrons. As a result we find a small AH contribution and a large SH one.

Expansion around the original Fermi surface: the topological Kondo Hamiltonian

Here we derive the $\mathbf{k}\cdot\mathbf{p}$ Hamiltonian describing the regions around $\boldsymbol{\kappa}$ and $\boldsymbol{\kappa}'$ where the Fermi surface of spin $\uparrow$ and $\downarrow$, respectively, conduction electrons is located. The analysis clarifies the topological origin of the hybridization gap. To start with we observe that the mean-field heavy Fermi liquid Hamiltonian reads:

$$H_\sigma(\mathbf{k}) = \begin{pmatrix} \lambda & J_K\Phi V_{\mathbf{k}} \\ J_K\Phi^* V^*_{\mathbf{k}} & \xi_{\mathbf{k}\sigma}\end{pmatrix}. \tag{37}$$

Expanding the form factor $V_{\mathbf{k}}$ and the dispersion $\xi_{\mathbf{k}\sigma}$ around $\boldsymbol{\kappa}$ we readily find:

$$H_\uparrow(\boldsymbol{\kappa}+\mathbf{k}) = \begin{pmatrix} \lambda & -\Delta_K(k_x - ik_y) \\ -\Delta_K(k_x+ik_y) & \hbar^2k^2/(2m_W) - \mu\end{pmatrix}, \tag{38}$$

and $H_\downarrow(\boldsymbol{\kappa}'+\mathbf{k}) = H^*_\uparrow(\boldsymbol{\kappa}-\mathbf{k})$. The crossing between the local moment χ and the c-electron dispersive band takes place of a circle with radius $k_c = \sqrt{2m_W(\mu+\lambda)}$ where the continuum model reduces to $H_\uparrow(\boldsymbol{\kappa}+\mathbf{k}_c) = -\Delta_K k_c(e^{i\theta}\tau^- + e^{-i\theta}\tau^+)$.

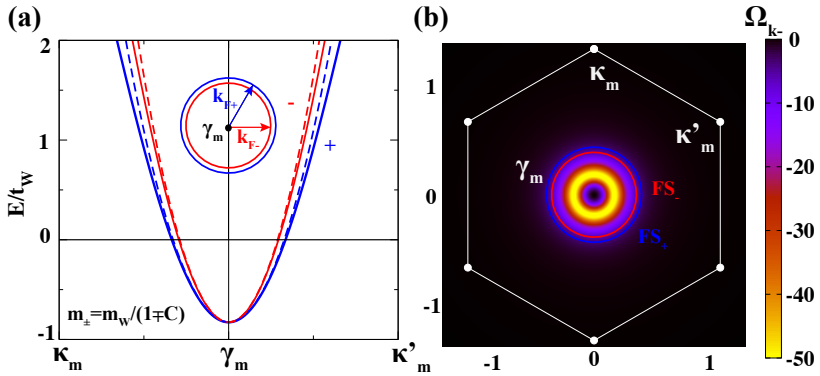

Figure S4. **Bandstructure and Berry curvature of the small Fermi surface magnetic state.** (a) Dispersion of the electrons close to the bottom of the conduction band. Dashed lines are obtained with the continuum Hamiltonian (19) while the solid ones are the lowest energy bands of the mean-field Hamiltonian (18). (b) Berry curvature around the origin of the magnetic Brillouin zone. Solid lines show the two Fermi surfaces. The calculations has been performed at doping $x = 0.08$, $J_K/t_W = 1$, $J_H/t_W = 0.025$ and magnetic field $h_W/t_W = 0.08$.

The interlayer Kondo hybridization lifts the degeneracy and induces winding in the two dimensional space associated with the interlayer degrees of freedom $\boldsymbol{\tau}$. The resulting Berry curvature can be readily obtained from the Kubo formula observing that the eigenvalues of Eq. (38) are described by the matrix $U(\mathbf{k}) = \exp[-i\varphi_{\mathbf{k}}(\mathbf{k}\times\boldsymbol{\tau})_z/2]$ with $\tan\varphi_{\mathbf{k}} = \Delta_K k/d_z$ and d_z projection of the Hamiltonian along τ^z. The integral gives quantized Chern number $C_\uparrow = -C_\downarrow = 1$. The model gives a topological Kondo metal which is adiabatically connected to a quantum Spin Hall Kondo insulator at filling 2.

The magnetic regime

We now turn our attention in the magnetic regime where only the c-electrons contribute to charge transport. The low-energy Hamiltonian is given in Eq. (19) and describes electrons with dispersion relation $\epsilon_{\mathbf{k}\lambda} = \hbar^2k^2/2m_\lambda$ shown in Fig. S4(a) and group velocity $\boldsymbol{v}_{\mathbf{k}\lambda} = \hbar\mathbf{k}/m_\lambda$ with $m_\lambda = m_W/[1-\lambda J_K|M|/(4t_W)]$ and $\lambda = \pm$. Under the assumption of a single transport time, i.e. momentum- and band-independent, we apply Eqs. (32) and (33) to find $\sigma_{xx} = e^2\tau x/\left(\sum_\lambda m_\lambda/2\right)$ and $\sigma_{xy}^{\rm Ohm} = e^3\tau^2Bx/\left(m_W\sum_\lambda m_\lambda/2\right)$. We now conclude our analysis considering the AHE contribution coming from the the Berry phase winding introduced by the $d_x(\mathbf{k})$ and $d_y(\mathbf{k})$ terms in Eq. (19). In the absence of an external magnetic field $M^z = 0$ and the eigenstates are simply $|u_{\mathbf{k}\pm}\rangle = (1, \pm e^{-2i\varphi_{\mathbf{k}}})\sqrt{2}$ with 2π-Berry phase around the origin of the magnetic Brillouin zone. A small Zeeman term opens a gap in the band structure and gives rise to a finite Berry curvature $\Omega_\pm(\mathbf{k})$:

$$\Omega_\pm(\mathbf{k}) = \pm\frac{64h^2k^2\eta^2}{\left[16k^4\eta^2 + \left(2h + \frac{m_\uparrow - m_\downarrow}{m_\uparrow m_\downarrow}k^2\right)^2\right]^{3/2}}, \tag{39}$$

where $\eta = 9J_KM^\parallel/8$ and $m_{\uparrow/\downarrow} = m_W/[1 \pm J_KM^z/(4t_W)]$. We notice that the Berry curvature is an even function of k, vanishes quadratically at $k = 0$ and takes its maximum value at finite momentum k. The maximum is located at $k^4_{\rm max} = h^2/(8\eta^2)$ for $M^z = 0$. The momentum space distribution in the magnetic moiré Brillouin zone is given in Fig. S4(b). We observe that from Eq. (39) the anomalous Hall conductivity is obtained as:

$$\sigma_{xy}^{\rm AH} = \frac{e^2}{2\pi h}\sum_\lambda\int d^2\mathbf{k}\Omega_\lambda(\mathbf{k})f(\epsilon_{\mathbf{k}\lambda} - \mu), \tag{40}$$

which in the zero temperature limit becomes:

$$\sigma_{xy}^{\rm AH} = \frac{e^2}{h}\int_{k_F^-}^{k_F^+} dk\, k\,\Omega_+(k) = \frac{e^2}{h}\frac{h[k^2(m_\downarrow - m_\uparrow) - 2hm_\uparrow m_\downarrow]}{\sqrt{16k^4\eta^2(m_\uparrow m_\downarrow)^2 + [k^2(m_\uparrow - m_\downarrow) + 2hm_\uparrow m_\downarrow]^2}}\Bigg|_{k_F^-}^{k_F^+}. \tag{41}$$

REFERENCES AND NOTES

1. T. Li, S. Jiang, B. Shen, Y. Zhang, L. Li, Z. Tao, T. Devakul, K. Watanabe, T. Taniguchi, L. Fu, J. Shan, K. F. Mak, Quantum anomalous hall effect from intertwined moiré bands, *Nature* **600**, 641–646 (2021).
2. Z. Tao, B. Shen, S. Jiang, T. Li, L. Li, L. Ma, W. Zhao, J. Hu, K. Pistunova, K. Watanabe, T. Taniguchi, T. F. Heinz, K. F. Mak, J. Shan, Valley-coherent quantum anomalous Hall state in AB-stacked MoTe2/WSe2 bilayers. arXiv:2208.07452 [cond-mat.mes-hall] (15 August 2022).
3. W. Zhao, K. Kang, L. Li, C. Tschirhart, E. Redekop, K. Watanabe, T. Taniguchi, A. Young, J. Shan, K. F. Mak, Realization of the Haldane Chern insulator in a moiré lattice. arXiv:2207.02312 [cond-mat.mes-hall] (5 July 2022).
4. T. Li, S. Jiang, L. Li, Y. Zhang, K. Kang, J. Zhu, K. Watanabe, T. Taniguchi, D. Chowdhury, L. Fu, J. Shan, K. F. Mak, Continuous mott transition in semiconductor moiré superlattices. *Nature* **597**, 350–354 (2021).
5. A. Ghiotto, E.-M. Shih, G. S. S. G. Pereira, D. A. Rhodes, B. Kim, J. Zang, A. J. Millis, K. Watanabe, T. Taniguchi, J. C. Hone, L. Wang, C. R. Dean, A. N. Pasupathy, Quantum criticality in twisted transition metal dichalcogenides. *Nature* **597**, 345–349 (2021)
6. H. Li, S. Li, E. C. Regan, D. Wang, W. Zhao, S. Kahn, K. Yumigeta, M. Blei, T. Taniguchi, K. Watanabe, S. Tongay, A. Zettl, M. F. Crommie, F. Wang, Imaging two-dimensional generalized wigner crystals. *Nature* **597**, 650–654 (2021).
7. F. Wu, T. Lovorn, E. Tutuc, A. H. MacDonald, Hubbard model physics in transition metal dichalcogenide moiré bands. *Phys. Rev. Lett.* **121**, 026402 (2018).
8. T. Devakul, V. Crépel, Y. Zhang, L. Fu, Magic in twisted transition metal dichalcogenide bilayers. *Nat. Commun.* **12**, 6730 (2021).
9. J. Zang, J. Wang, J. Cano, A. J. Millis, Hartree-fock study of the moiré hubbard model for twisted bilayer transition metal dichalcogenides. *Phys. Rev. B* **104**, 075150 (2021).
10. J. Zang, J. Wang, J. Cano, A. Georges, A. J. Millis, Dynamical mean-field theory of moiré bilayer transition metal dichalcogenides: Phase diagram, resistivity, and quantum criticality. *Phys. Rev. X* **12**, 021064 (2022).
11. J. Wang, J. Zang, J. Cano, A. J. Millis, Staggered pseudo magnetic field in twisted transition metal dichalcogenides: Physical origin and experimental consequences. *Phys. Rev. Res.* **5**, L012005 (2023).
12. A. Wietek, J. Wang, J. Zang, J. Cano, A. Georges, A. Millis, Tunable stripe order and weak superconductivity in the Moiré Hubbard model. *Phys. Rev. Res.* **4**, 043048 (2022).

13. H. Pan, M. Xie, F. Wu, S. D. Sarma, Topological phases in AB-stacked $MoTe_2/WSe_2$: $\square_2$ topological insulators, chern insulators, and topological charge density waves. *Phys. Rev. Lett.* **129**, 056804 (2022).
14. T. Devakul, L. Fu, Quantum anomalous hall effect from inverted charge transfer gap. *Phys. Rev. X* **12**, 021031 (2022).
15. Y.-M. Xie, C.-P. Zhang, J.-X. Hu, K. F. Mak, K. T. Law, Valley-polarized quantum anomalous Hall state in Moiré $MoTe_2/WSe_2$ heterobilayers. *Phys. Rev. Lett.* **128**, 026402 (2022).
16. Y.-M. Xie, C.-P. Zhang, K. T. Law, Topological $p_x + ip_y$ inter-valley coherent state in Moiré $MoTe_2/WSe_2$ heterobilayers. arXiv:2206.11666 [cond-mat.mtrl-sci] (23 June 2022).
17. M. Xie, H. Pan, F. Wu, S. D. Sarma, Nematic excitonic insulator in transition metal dichalcogenide moiré heterobilayers. arXiv:2206.12427 [cond-mat.str-el] (24 June 2022).
18. Z. Dong, Y.-H. Zhang, Excitonic Chern insulator and kinetic ferromagnetism in $MoTe_2/WSe_2$ moiré bilayer. *Phys. Rev. B* **107**, L081101 (2023).
19. M. Davydova, Y. Zhang, L. Fu, Itinerant spin polaron and metallic ferromagnetism in semiconductor moiré superlattices. arXiv:2206.01221 [cond-mat.str-el] (2 June 2022).
20. G.-B. Liu, W.-Y. Shan, Y. Yao, W. Yao, D. Xiao, Three-band tight-binding model for monolayers of group-vib transition metal dichalcogenides. *Phys. Rev. B* **88**, 085433 (2013).
21. A. Kormányos, G. Burkard, M. Gmitra, J. Fabian, V. Zólyomi, N. D. Drummond, V. Fal'ko, **k·p** theory for two-dimensional transition metal dichalcogenide semiconductors. *2D Materials* **2**, 022001 (2015).
22. M. Yi, D. H. Lu, R. Yu, S. C. Riggs, J.-H. Chu, B. Lv, Z. K. Liu, M. Lu, Y.-T. Cui, M. Hashimoto, S.-K. Mo, Z. Hussain, C. W. Chu, I. R. Fisher, Q. Si, Z.-X. Shen, Observation of temperature-induced crossover to an orbital-selective Mott phase in $A_xFe_{2-y}Se_2$ (A = K, rb) superconductors. *Phys. Rev. Lett.* **110**, 067003 (2013).
23. M. Yi, Z.-K. Liu, Y. Zhang, R. Yu, J.-X. Zhu, J. Lee, R. Moore, F. Schmitt, W. Li, S. Riggs, J.-H. Chu, B. Lv, J. Hu, M. Hashimoto, S.-K. Mo, Z. Hussain, Z. Mao, C. Chu, I. Fisher, Q. Si, Z.-X. Shen, D. Lu, Observation of universal strong orbital-dependent correlation effects in iron chalcogenides. *Nat. Commun.* **6**, 7777 (2015).
24. Y. J. Pu, Z. C. Huang, H. C. Xu, D. F. Xu, Q. Song, C. H. P. Wen, R. Peng, D. L. Feng, Temperature-induced orbital selective localization and coherent-incoherent crossover in single-layer FeSe/Nb : $BaTiO_3/KTaO_3$. *Phys. Rev. B* **94**, 115146 (2016).
25. R. Yu, Q. Si, Orbital-selective mott phase in multiorbital models for alkaline iron selenides $\mathbf{K}_{1-x}Fe_{2-y}Se_2$. *Phys. Rev. Lett.* **110**, 146402 (2013).

26. M. Yi, Y. Zhang, Z.-X. Shen, D. Lu, Role of the orbital degree of freedom in iron-based superconductors. *npj Quant. Mater.* **2**, 57 (2017).
27. Y. Zhang, T. Devakul, L. Fu, Spin-textured chern bands in AB-stacked transition metal dichalcogenide bilayers. *Proc. Natl. Acad. Sci. U.S.A.* **118**, e2112673118 (2021).
28. Z.-D. Song, B. A. Bernevig, MATBG as topological heavy fermion: I. Exact mapping and correlated insulators. arXiv:2111.05865 [cond-mat.str-el] (10 November 2021).
29. A. Ramires, J. L. Lado, Emulating heavy fermions in twisted trilayer graphene. *Phys. Rev. Lett.* **127**, 026401 (2021).
30. A. Dalal, J. Ruhman, Orbitally selective mott phase in electron-doped twisted transition metal-dichalcogenides: A possible realization of the kondo lattice model. *Phys. Rev. Res.* **3**, 043173 (2021).
31. A. Kumar, N. C. Hu, A. H. MacDonald, A. C. Potter, Gate-tunable heavy fermion quantum criticality in a moiré kondo lattice. *Phys. Rev. B* **106**, L041116 (2022).
32. See the Supplementary Materials for details on the continuum and the tight binding Hamiltonian, the Schrieffer-Wolff transformation, and the mean-field theory of Abrikosov fermions.
33. J. R. Schrieffer, P. A. Wolff, Relation between the anderson and kondo hamiltonians. *Phys. Rev.* **149**, 491–492 (1966).
34. A. H. MacDonald, S. M. Girvin, D. Yoshioka, $\frac{t}{U}$ expansion for the Hubbard model. *Phys. Rev. B* **37**, 9753 (1988).
35. P. Coleman, N. Andrei, Kondo-stabilised spin liquids and heavy fermion superconductivity. *J. Phys. Condens. Matter* **1**, 4057–4080 (1989).
36. T. Senthil, M. Vojta, S. Sachdev, Weak magnetism and non-fermi liquids near heavy-fermion critical points. *Phys. Rev. B* **69**, 035111 (2004).
37. J. Pixley, R. Yu, Q. Si, Quantum phases of the shastry-sutherland kondo lattice: Implications for the global phase diagram of heavy-fermion metals. *Phys. Rev. Lett.* **113**, 176402 (2014).
38. S. Doniach, The Kondo lattice and weak antiferromagnetism. *Physica B+C* **91**, 231 (1977).
39. M. Oshikawa, Topological approach to luttinger's theorem and the fermi surface of a kondo lattice. *Phys. Rev. Lett.* **84**, 3370–3373 (2000).
40. C. L. Kane, E. J. Mele, Quantum spin hall effect in graphene. *Phys. Rev. Lett.* **95**, 226801 (2005).
41. M. Dzero, K. Sun, V. Galitski, P. Coleman, Topological kondo insulators. *Phys. Rev. Lett.* **104**, 106408 (2010).

42. M. Dzero, J. Xia, V. Galitski, P. Coleman, Topological kondo insulators. *Annu. Rev. Condens. Matter Phys.* **7**, 249–280 (2016).
43. S. Wolgast, Ç. Kurdak, K. Sun, J. W. Allen, D.-J. Kim, Z. Fisk, Low-temperature surface conduction in the kondo insulator SmB_6. *Phys. Rev. B* **88**, 180405 (2013).
44. D. J. Kim, S. Thomas, T. Grant, J. Botimer, Z. Fisk, J. Xia, Surface hall effect and nonlocal transport in SmB_6: Evidence for surface conduction. *Sci. Rep.* **3**, 3150 (2013).
45. M. Neupane, N. Alidoust, S.-Y. Xu, T. Kondo, Y. Ishida, D. J. Kim, C. Liu, I. Belopolski, Y. J. Jo, T.-R. Chang, H.-T. Jeng, T. Durakiewicz, L. Balicas, H. Lin, A. Bansil, S. Shin, Z. Fisk, M. Z. Hasan, Surface electronic structure of the topological kondo-insulator candidate correlated electron system SmB_6. *Nat. Commun.* **4**, 2991 (2013).
46. N. Xu, P. K. Biswas, J. H. Dil, R. S. Dhaka, G. Landolt, S. Muff, C. E. Matt, X. Shi, N. C. Plumb, M. Radović, E. Pomjakushina, K. Conder, A. Amato, S. V. Borisenko, R. Yu, H.-M. Weng, Z. Fang, X. Dai, J. Mesot, H. Ding, M. Shi, Direct observation of the spin texture in SmB6 as evidence of the topological kondo insulator. *Nat. Commun.* **5**, 4566 (2014).
47. C. Robert, H. Dery, L. Ren, D. Van Tuan, E. Courtade, M. Yang, B. Urbaszek, D. Lagarde, K. Watanabe, T. Taniguchi, T. Amand, X. Marie, Measurement of conduction and valence bands *g*-factors in a transition metal dichalcogenide monolayer. *Phys. Rev. Lett.* **126**, 067403 (2021).
48. N. P. Ong, Geometric interpretation of the weak-field hall conductivity in two-dimensional metals with arbitrary fermi surface. *Phys. Rev. B* **43**, 193–201 (1991).
49. F. D. M. Haldane, Berry curvature on the fermi surface: Anomalous hall effect as a topological fermi-liquid property. *Phys. Rev. Lett.* **93**, 206602 (2004).
50. D. Chowdhury, I. Sodemann, T. Senthil, Mixed-valence insulators with neutral fermi surfaces. *Nat. Commun.* **9**, 1766 (2018).
51. L. B. Ioffe, A. I. Larkin, Gapless fermions and gauge fields in dielectrics. *Phys. Rev. B* **39**, 8988–8999 (1989).
52. S. Paschen, T. Lühmann, S. Wirth, P. Gegenwart, O. Trovarelli, C. Geibel, F. Steglich, P. Coleman, Q. Si, Hall-effect evolution across a heavy-fermion quantum critical point. *Nature* **432**, 881–885 (2004).
53. S. Friedemann, N. Oeschler, S. Wirth, C. Krellner, C. Geibel, F. Steglich, S. Paschen, S. Kirchner, Q. Si, Fermi-surface collapse and dynamical scaling near a quantum-critical point. *Proc. Natl. Acad. Sci. U.S.A.* **107**, 14547–14551 (2010).

54. S. Friedemann, S. Wirth, N. Oeschler, C. Krellner, C. Geibel, F. Steglich, S. MaQuilon, Z. Fisk, S. Paschen, G. Zwicknagl, Hall effect measurements and electronic structure calculations on $YbRh_2$ Si_2 and its reference compounds $LuRh_2Si_2$ and $Ybir_2Si_2$. *Phys. Rev. B* **82**, 035103 (2010).
55. W. Ding, S. Grefe, S. Paschen, Q. Si, Anomalous hall effect and quantum criticality in geometrically frustrated heavy fermion metals. arXiv:1507.07328 [cond-mat.str-el] (27 July 2015).
56. W. Zhao, B. Shen, Z. Tao, Z. Han, K. Kang, K. Watanabe, T. Taniguchi, K. F. Mak, J. Shan, Gate-tunable heavy fermions in a moiré Kondo lattice. arXiv:1507.07328 [cond-mat.str-el] (1 November 2022).
57. V. Crépel, L. Fu, Spin-triplet superconductivity from excitonic effect in doped insulators. *Proc. Natl. Acad. Sci. U.S.A.* **119**, e2117735119 (2022).